Letter

Dual topological characterization of non-Hermitian Floquet phases

Longwen Zhou,[1,*] Yongjian Gu,[1] and Jiangbin Gong[2,†]

[1]*Department of Physics, College of Information Science and Engineering, Ocean University of China, Qingdao 266100, China*

[2]*Department of Physics, National University of Singapore, Singapore 117543*

(Received 5 October 2020; accepted 7 January 2021; published 21 January 2021)

Non-Hermiticity is expected to add far more physical features to the already rich Floquet topological phases of matter. Nevertheless, a systematic approach to characterize non-Hermitian Floquet topological matter is still lacking. In this work we introduce a dual scheme to characterize the topology of non-Hermitian Floquet systems in momentum space and in real space using a piecewise quenched nonreciprocal Su-Schrieffer-Heeger model for our case studies. Under the periodic boundary condition, topological phases are characterized by a pair of experimentally accessible winding numbers that make jumps between integers and half integers. Under the open boundary condition, a Floquet version of the so-called open boundary winding number is found to be integers and can predict the number of pairs of zero and π Floquet edge modes coexisting with the non-Hermitian skin effect. Our results indicate that a dual characterization of non-Hermitian Floquet topological matter is necessary and also feasible because the formidable task of constructing the celebrated generalized Brillouin zone for non-Hermitian Floquet systems with multiple hopping length scales can be avoided. This work hence paves a way for further studies of non-Hermitian physics in nonequilibrium systems.

DOI: 10.1103/PhysRevB.103.L041404

Introduction. Floquet topological phases, as created by time-periodic modulations, have been an experimental reality in both synthetic metamaterials [1–4] and actual condensed-matter systems [5,6]. One genuinely promising feature of such nonequilibrium topological phases is that they may accommodate an arbitrary number of topological edge modes [7], e.g., the coexistence of many chiral edge modes to enhance robust transport [8,9] and on-demand generation of multiple dispersionless edge modes [10–12] for encoding and processing quantum information [13,14]. To further explore far-reaching possibilities offered by Floquet topological matter, it is timely and potentially fruitful to introduce non-Hermiticity to periodically driven lattice systems.

The interplay between periodic driving and non-Hermiticity is expected to be rich [15–17] and has already led to some encouraging findings [18–34]. Two aspects of non-Hermitian Floquet matter are worthy of special attention. First, the exceptional topology [35–37] in the complex Floquet band structure can potentially create even richer topological phases absent in Hermitian cases. Independent of other topological aspects of Floquet bands, characterizing and experimentally detecting Floquet exceptional topology are of general interest. Second, the so-called non-Hermitian skin effect (NHSE) [38–45], which corresponds to the pileup of bulk states at the edges of a non-Hermitian lattice, must also be well addressed for a topological characterization aiming at predicting the emergence of many topological edge modes, localized not because of NHSE but topological localization [46]. Remarkably, the very main reason of why Floquet topological phases can be so rich, namely, the emergent/effective hoppings across different and extended hopping ranges [10] in the same system, presents a severe challenge in analyzing the NHSE with the celebrated generalized Brillouin zone (GBZ) treatment [39–49]. That is, the GBZ would be too hard to be computationally constructed in Floquet systems with the coexistence of many different length scales [50].

Here we propose a dual topological characterization scheme to investigate a representative and simple class of non-Hermitian Floquet matter protected by chiral symmetry, in both momentum space and real space. Under the periodic boundary condition (PBC), the exceptional topology in the Floquet bands yields a phase diagram characterized by two species of winding numbers depicting Floquet effective Hamiltonians in two time frames, with the winding numbers being tunable without a bound and alternating between integers and half integers. These intriguing topological phases correspond to gap closing and reopening at eigenphase zero or π and can be directly probed in experiments. Under the open-boundary condition (OBC), more complications of topological characterization arise because an unlimited number of topological edge modes at eigenphases zero and π can coexsit with NHSEs. We propose a Floquet version of the so-called open-boundary winding numbers (OBWNs) [40] in real space. Two types of OBWNs are advocated, being always integers, and they precisely match the number of pairs of the two different types of Floquet edge modes. The OBWNs jump only when the spectral gap under OBC closes and reopens. As further elaborated below, the topological characterization in momentum and that in real space are different but also related, thus indicating the necessity of a dual approach for a complete picture of non-Hermitian Floquet topological phases.

*zhoulw13@u.nus.edu
†phygj@nus.edu.sg

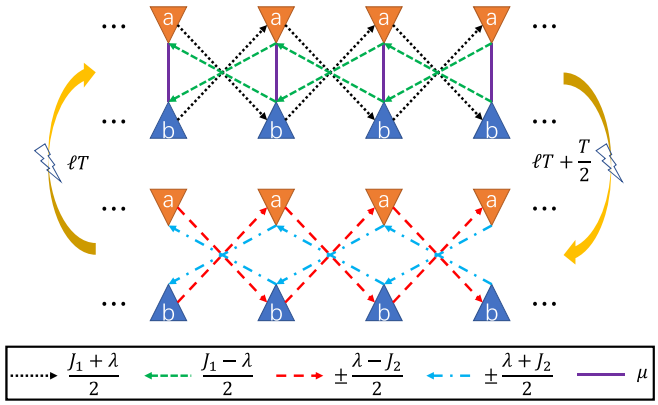

FIG. 1. Schematic illustration of the periodically quenched NHSSH model. Each unit cell contains two sublattices, which are coupled by the intracell hopping amplitude μ. The intercell hopping amplitudes in the first and second halves of the driving period are $\frac{J_1\pm\lambda}{2}$ and $\pm\frac{\lambda\pm J_2}{2}$. The lightning symbols denote quenches applied in the middle/end of each driving period, after which the lattice is switched from the configuration of the upper/lower to the lower/upper array of the figure.

It is also tempting to view the seen differences as evidence of a needed breakdown of the old concept of bulk-edge correspondence.

Model. To make our theoretical considerations more explicit, we start with a non-Hermitian Su-Schrieffer-Heeger (NHSSH) model [40] under periodic quenches. In momentum space the Hamiltonian of the model takes the form

$$H(k,t)=\begin{cases}H_x(k)=h_x(k)\sigma_x & t\in\left[\ell T,\ell T+\frac{T}{2}\right)\\ H_y(k)=h_y(k)\sigma_y & t\in\left[\ell T+\frac{T}{2},\ell T+T\right)\end{cases}. \quad (1)$$

Here the quasimomentum $k\in[-\pi,\pi)$, $\ell\in\mathbb{Z}$, T is the driving period, and $\sigma_{x,y,z}$ are Pauli matrices acting on the sublattice degrees of freedom. The components of the Hamiltonian are given by $h_x(k)=\mu+J_1\cos k+i\lambda\sin k$ and $h_y(k)=J_2\sin k+i\lambda\cos k$. μ and $\frac{J_1+J_2}{2}$ are the intracell and intercell hopping amplitudes of the SSH model. The non-Hermiticity is introduced by asymmetric hoppings $\frac{J_1-J_2}{2}\pm i\frac{\lambda}{2}$ between the two sublattices. An illustration of the model is given in Fig. 1.

We set $\hbar=1$ throughout and the driving period $T=2$. Following Eq. (1), the Floquet operator depicting the time evolution is $U(k)=e^{-ih_y(k)\sigma_y}e^{-ih_x(k)\sigma_x}$. Referring to the established topological characterization of one-dimensional (1D) Floquet systems [11,51,52], we introduce a pair of symmetric time frames in which $U(k)$ take the forms $U_1(k)=e^{-i\frac{h_x(k)}{2}\sigma_x}e^{-ih_y(k)\sigma_y}e^{-i\frac{h_x(k)}{2}\sigma_x}=e^{-iH_1(k)}$ and $U_2(k)=e^{-i\frac{h_y(k)}{2}\sigma_y}e^{-ih_x(k)\sigma_x}e^{-i\frac{h_y(k)}{2}\sigma_y}=e^{-iH_2(k)}$. Since $U(k)$ and $U_{1,2}(k)$ are related by similarity transformations, they share the same Floquet eigenphase spectrum $E(k)$, which can be obtained by solving $H_\alpha(k)|\psi_\alpha^\pm(k)\rangle=\pm E(k)|\psi_\alpha^\pm(k)\rangle$ for $\alpha=1,2$ [53]. With Taylor expansions of $e^{-i\frac{h_{x,y}(k)}{2}\sigma_{x,y}}$, $e^{-ih_{x,y}(k)\sigma_{x,y}}$, and combining the resulting terms, we find the effective Hamiltonians

$$H_\alpha(k)=h_{\alpha x}(k)\sigma_x+h_{\alpha y}(k)\sigma_y,\quad \alpha=1,2. \quad (2)$$

$H_\alpha(k)$ possesses the chiral (sublattice) symmetry $\mathcal{S}=\sigma_z$, time-reversal symmetry $\mathcal{T}=\sigma_0$, and particle-hole symmetry $\mathcal{C}=\sigma_z$, i.e., $\mathcal{S}H_\alpha(k)\mathcal{S}=-H_\alpha(k)$, $\mathcal{T}H_\alpha^*(k)\mathcal{T}^{-1}=H_\alpha(-k)$, and $\mathcal{C}H_\alpha^*(k)\mathcal{C}^{-1}=-H_\alpha(-k)$, where σ_0 denotes the 2×2 identity matrix. The system under study hence belongs to the symmetry class BDI [54–56]. The symmetry $\mathcal{S}$ ensures that the eigenvalues of $H_\alpha(k)$ appear in positive-negative pairs on the complex plane, yielding the topological protection of Floquet edge modes at $E=0,\pi$. In addition, $H_\alpha(k)$ also lacks the inversion symmetry, indicating the existence of NHSEs [55].

Momentum-space characterization. Since $H_\alpha(k)$ possesses the chiral symmetry, we proceed to use the following winding number w_α [17]:

$$w_\alpha=\int_{-\pi}^{\pi}\frac{dk}{2\pi}\partial_k\phi_\alpha(k),\quad \alpha=1,2, \quad (3)$$

where the winding angle $\phi_\alpha(k)\equiv\arctan[h_{\alpha y}(k)/h_{\alpha x}(k)]$. w_α counts the number of times the angle $\phi_\alpha(k)$ changes over 2π as the quasimomentum k sweeps across the first Brillouin zone (BZ). Thus this topological invariant is based entirely from the momentum-space effective Hamiltonian in two different time frames. Notably, w_α is highly nontrivial because $h_{\alpha x}(k)$ and $h_{\alpha y}(k)$ are complex functions. Furthermore, the imaginary part of $\phi_\alpha(k)$ has no contribution to the integral over k, and w_α is hence real [19,57]. More importantly, except for some special initial states, w_α thus defined can be measured dynamically by averaging some spin textures over a sufficiently long time [17,19].

Back to the original time frame, we can now introduce two species of invariants to characterize the bulk topological properties. With the winding numbers (w_1,w_2), we define topological invariants

$$w_0=\frac{w_1+w_2}{2},\qquad w_\pi=\frac{w_1-w_2}{2}. \quad (4)$$

As confirmed below, (w_0,w_π) are respectively protected by Floquet band gaps around eigenphases zero and π. Interestingly, the system parameters chosen in previous studies [17–20] happened to guarantee that always integer values of (w_0,w_π) can be obtained. However, we discover that in more general situations, w_0 or w_π can take half-integer values, small or large. In particular, half integer w_π indicates the emergence of exceptional topology due to the gap closing at $E=\pi$, which is absent in static systems. Such half-integer windings should not be connected with the number of possible Floquet edge modes (because there cannot be a half pair of topological edge modes for the symmetry class under consideration). Nevertheless, since (w_0,w_π) can be measured from dynamical spin textures [17,19,58] and are robust to perturbations that preserve the chiral symmetry, they do present together a momentum-space topological characterization.

As a typical case, we present the topological phase diagram of the periodically quenched NHSSH model versus the hopping parameters in Fig. 2. The values of w_0 and w_π are obtained from Eqs. (3) and (4), and are marked explicitly in each region of the left and right panels. Different non-Hermitian Floquet topological phases are distinguished by their colors. It is seen that with the change of J_1 and μ, the system undergoes a series of topological phase transitions, which are accompanied by quantized or half-quantized jumps of w_0 or w_π. Furthermore, with the increase of J_1, a monotonous

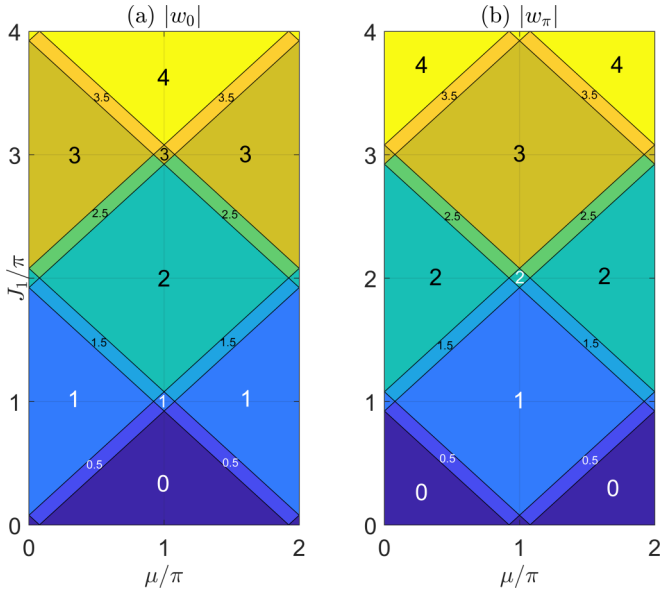

FIG. 2. Bulk topological phase diagram of the periodically quenched NHSSH model vs hopping parameters μ and J_1. Other system parameters are $(J_2, \lambda) = (0.5\pi, 0.25)$. Each region with a uniform color denotes a topological phase characterized by the winding numbers (w_0, w_π). The solid lines between different regions are boundaries between distinct non-Hermitian Floquet topological phases. The values of w_0 and w_π for each phase are denoted explicitly in panels (a) and (b).

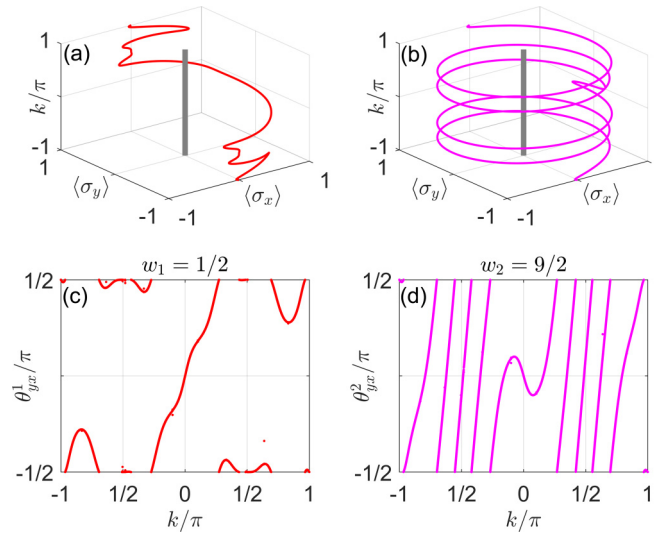

FIG. 3. Spin textures and dynamic winding angles of the periodically quenched NHSSH model in time frames $\alpha = 1$ [panels (a, c)] and $\alpha = 2$ [panels (b, d)]. System parameters are $(J_1, J_2, \mu, \lambda) = (2.4\pi, 0.5\pi, 0.4\pi, 0.25)$, and evolutions are averaged over 500 driving periods to generate the winding angles $\theta^{1,2}_{yx}$ in panels (c, d). In the panel (a) [(b)], the red (magenta) points denote $(\langle\sigma_x\rangle, \langle\sigma_y\rangle)$ in the first (second) time frame. The gray solid line denotes the origin of $\langle\sigma_x\rangle$-$\langle\sigma_y\rangle$ plane. In panel (c) [(d)], the red (magenta) points correspond to the dynamic winding angles θ^1_{yx} (θ^2_{yx}) in time frame 1 (2) [19]. The values of (w_1, w_2) are also shown in panels (c, d).

increase of the values of w_0 or w_π across each transition is observed, yielding non-Hermitian Floquet states characterized by large integers or large half integers for both species of winding numbers. These intriguing phases are unique to non-Hermitian Floquet systems [53].

To digest the physical meanings of the half-integer winding numbers, we present the long-time averaged spin textures and dynamic winding numbers [19] for a typical situations in Fig. 3, where the panels (a) and (b) show the trajectories of spin vector $(\langle\sigma_x\rangle, \langle\sigma_y\rangle)$ versus the quasimomentum k in the time frame $\alpha = 1$ and 2. The average $\langle\cdots\rangle$ is taken with respect to the right eigenvector $|\psi^+_\alpha(k)\rangle$ of $H_\alpha(k)$. The gray thick lines highlight the origin of the $\langle\sigma_x\rangle$-$\langle\sigma_y\rangle$ plane, which satisfy the equation $(\langle\sigma_x\rangle, \langle\sigma_y\rangle) = 0$ at all $k \in [-\pi, \pi)$. In Figs. 3(a) and 3(b), we see that the projection of $(\langle\sigma_x\rangle, \langle\sigma_y\rangle)$ on the $\langle\sigma_x\rangle$-$\langle\sigma_y\rangle$ plane contains an integer plus a half circle, which indicates the presence of half-integer winding numbers. For example, starting at $(\langle\sigma_x\rangle, \langle\sigma_y\rangle) = (0, -1)$, the vector $(\langle\sigma_x\rangle, \langle\sigma_y\rangle)$ rotates counterclockwise around the origin over 4.5 cycles, ending at $(\langle\sigma_x\rangle, \langle\sigma_y\rangle) = (0, 1)$ when k sweeps from $-\pi$ to π, as shown in Fig. 3(b). These half-integer windings are caught by the winding angles of dynamic spin textures $\theta^{1,2}_{yx}$, as shown in panels (c, d) of Fig. 3 (see Ref. [19] for the definition and calculation of the dynamic winding angles), where the net increments of $\theta^{1,2}_{yx}$ across the first BZ are odd-integer multiples of π, yielding half-quantized integers after being divided by 2π. In Ref. [19] it was proven that $(\theta^1_{yx}/2\pi, \theta^2_{yx}/2\pi)$ are equal to (w_1, w_2) defined in Eq. (3). Therefore, if $(\theta^1_{yx} + \theta^2_{yx})/(2\pi)$ or $(\theta^1_{yx} - \theta^2_{yx})/(2\pi)$ happens to be an odd integer, we obtain a half-quantized invariant w_0 or w_π according to Eq. (4). Thus, the half-integer quantization of (w_0, w_π) can also be dynamically extracted from time-averaged spin textures [53].

Qualitatively, the half windings of w_1 and w_2 may be traced back to the branch switch of the two Floquet bands when k varies from $-\pi$ to π [43]. Together with the above-mentioned symmetry between the upper and lower complex plane of the Floquet spectrum, the band switch (braiding) indicates that there is necessarily windings of the Floquet spectral flow on the complex plane, thus signaling the existence of NHSE [41–45,48]. To treat the possible coexistence of many Floquet edge modes with NHSE, we next move on to real-space characterization.

Real-space topological characterization. The above-obtained large winding numbers in momentum space already indicate the existence of multiple scales of hopping in the Floquet effective Hamiltonians. In such situations, construction of a GBZ to treat NHSE is not practical. This motivates us to extend the OBWN previously for static non-Hermitian systems [40] to non-Hermitian Floquet lattices.

We first define the $\mathcal{Q}$ matrix [53] in a time frame α as $\mathcal{Q}_\alpha = \sum_n (|\psi^+_{\alpha n}\rangle\langle\tilde{\psi}^+_{\alpha n}| - |\psi^-_{\alpha n}\rangle\langle\tilde{\psi}^-_{\alpha n}|)$. The right (left) Floquet eigenvectors $|\psi^\pm_{\alpha n}\rangle$ ($\langle\tilde{\psi}^\pm_{\alpha n}|$) satisfy the eigenvalue equations $U_\alpha|\psi^\pm_{\alpha n}\rangle = e^{-i(\pm E_n)}|\psi^\pm_{\alpha n}\rangle$ $[\langle\tilde{\psi}^\pm_{\alpha n}|U_\alpha = \langle\tilde{\psi}^\pm_{\alpha n}|e^{-i(\pm E_n)}]$, with $\pm E_n$ being the eigenphases. U_α is given by the real-space representation of $U_\alpha(k)$. With $\mathcal{Q}_\alpha$, one can construct the Floquet OBWN as

$$\nu_\alpha = \frac{1}{L_B}\mathrm{Tr}_B(\mathcal{S}\mathcal{Q}_\alpha[\mathcal{Q}_\alpha, \mathcal{N}]). \tag{5}$$

$\mathcal{S} = \mathbb{I}_{N\times N} \otimes \sigma_z$ is the chiral symmetry operator. $\mathcal{N}$ is the position operator of unit cells. N is the total number of unit cells. L_B and Tr_B share the same physical meanings as in the static version of OBWN [40,53,59–62]. That is, with the system decomposed into a bulk region and two edge regions around the left and right boundaries, the trace Tr_B is taken over the bulk region, which contains L_B lattice sites. Further, for a lattice of L sites, the length of each edge region is $L_E = (L - L_B)/2$. Though we make no attempt to construct a GBZ (which cannot be done), ν_α thus defined should, just as expected from the static case [40], essentially yield a winding number of the effective Hamiltonian $H_\alpha(k)$ in the αth time frame along the underlying GBZ. Finally, as one essential step in our treatment and in analogy to the definition of (w_0, w_π) in Eq. (4), we define two types of OBWNs of a 1D non-Hermitian Floquet system as

$$\nu_0 = \frac{\nu_1 + \nu_2}{2}, \qquad \nu_\pi = \frac{\nu_1 - \nu_2}{2}. \tag{6}$$

$(\nu_0, \nu_\pi) \in \mathbb{Z} \times \mathbb{Z}$ defined above serve as two new topological invariants arising from our real-space characterization for Floquet systems. We present below compelling evidence that this OBC characterization works properly because they can predict the numbers of topologically protected modes at eigenphases zero and π, denoted as (n_0, n_π), through the bulk-edge correspondence relations $(n_0, n_\pi) = 2(|\nu_0|, |\nu_\pi|)$.

Let us now compare the Floquet eigenphase spectrum of the periodically quenched NHSSH model under the PBC and OBC. To reveal the gap closing-reopening points clearly, we introduce gap functions $\Delta_0 = |E|/\pi$ and $\Delta_\pi = \sqrt{(|\mathrm{Re}E| - \pi)^2 + (\mathrm{Im}E)^2}/\pi$. It is clear that the Floquet spectrum become gapless at $E = 0$ ($E = \pi$) if $\Delta_0 = 0$ ($\Delta_\pi = 0$), where a phase transition occurs. In Fig. 4 we show (Δ_0, Δ_π) of our model versus the hopping amplitude J_1 under both the PBC and OBC in a lattice of $L = 400$ sites. The spectrum under PBC (in blue solid and green dotted lines) and OBC (in gray solid and red dotted lines) are expectedly similar in regimes far from gap closing points but clearly different near the gapless points. For example, at $J_1 = 0.4\pi$, one sees a phase transition with $\Delta_0 = 0$ under the OBC, after which a pair of edge modes with $E = 0$ emerges [63]. However, the spectrum under PBC suggests two consecutive transitions at $J_1 < 0.4\pi$ and $J_1 > 0.4\pi$. In between, there is a bulk topological phase with winding number $w_0 = 1/2$ according to Eqs. (3) and (4). Figure 4 presents many other similar regimes where the momentum-space topological invariants differ from the OBC winding numbers by 1/2. Such a clear distinction between the Floquet spectrum under PBC and OBC indicates the presence of NHSEs and breakdown of the bulk-edge correspondence [53].

We next compute (ν_0, ν_π) following Eqs. (5) and (6). The results are also presented in Fig. 4, where the numbers of zero and π Floquet edge modes are denoted. We see that the (ν_0, ν_π) take integer values within each non-Hermitian Floquet topological phase and undergo quantized jumps when J_1 is tuned through a topological phase transition point, where we have $\Delta_0 = 0$ or $\Delta_\pi = 0$ under OBC. Within each topological phase, (ν_0, ν_π) correctly count the numbers of zero and π edge modes, thus verifying the bulk-edge correspondence of our system albeit the existence of NHSEs. Besides, with

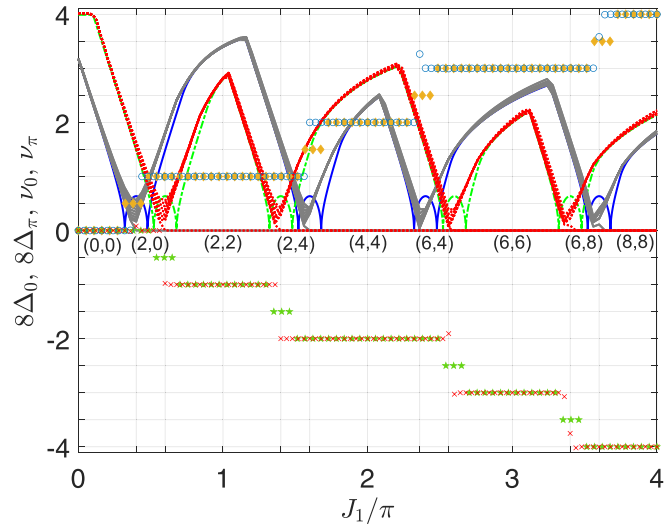

FIG. 4. Gap functions Δ_0 (blue and gray solid lines), Δ_π (red and green dotted lines), OBWNs ν_0 (circles), ν_π (crosses), and PBC winding numbers w_0 (diamonds), w_π (pentagrams) of the model. System parameters are $(\mu, J_2, \lambda) = (0.4\pi, 0.5\pi, 0.25)$. Phase transitions under OBC happen at $J_1 = (0.4\pi, 0.6\pi, 1.4\pi, 1.6\pi, 2.4\pi, 2.6\pi, 3.4\pi, 3.6\pi)$, denoted by the ticks along the horizontal axis. Only the first 20 smallest values of (Δ_0, Δ_π) under OBC are shown for clear illustrations. The numbers of zero and π Floquet edge modes are denoted below the horizontal axis.

the increase of J_1, almost monotonic increases in (ν_0, ν_π) and in the numbers of edge modes (n_0, n_π) are observed. This verifies again the enormous potential of Floquet engineering in realizing non-Hermitian Floquet states of matter with in principle unbounded topological invariants available and hence as many topological edge modes as we wish.

Summary. We have introduced a powerful dual scheme to characterize non-Hermitian Floquet topological matter, as illustrated by a simple periodically quenched NHSSH model. Rich non-Hermitian Floquet phases under PBC are characterized by two species of topological invariants that can be experimentally measured. The half-integer topological invariants associated with both zero and π gaps are identified as a general feature of exceptional topology in Floquet systems. Under the OBC, topological edge modes pinned at eigenphases zero and π can be generated in large numbers, together with NHSEs. We have found two OBWNs that can be used to characterize the Floquet topological phases in real space, thus avoiding the formidable task of constructing a GBZ. Interestingly, we now have two nonequivalent topological descriptions of the same Floquet system, with each of them necessary on its own right. Their differences also constitute a fascinating example of the breakdown of conventional bulk-edge correspondence (but well restored by OBWNs we proposed here). This work have thus laid a necessary and timely stage for further understanding and use of non-Hermitian Floquet phases for topologically based applications. In future work it would be interesting to extend our framework to higher-dimensional, disordered, and many-body non-Hermitian Floquet systems, in which the concept of GBZ does not apply in general.

Acknowledgments. The authors acknowledge Lee Ching Hua and Li Linhu for helpful comments. L.Z. is supported by the National Natural Science Foundation of China (Grant No. 11905211), the China Postdoctoral Science Foundation (Grant No. 2019M662444), the Fundamental Research Funds for the Central Universities (Grant No. 841912009), the Young Talents Project at Ocean University of China (Grant No. 861801013196), and the Applied Research Project of Postdoctoral Fellows in Qingdao (Grant No. 861905040009). J.G. acknowledges support from Singapore National Research Foundation Grant No. NRF- NRFI2017-04 (WBS No. R-144-000-378-281). Y.G. acknowledges support from the National Natural Science Foundation of China (Grant No. 61575180).

[1] M. C. Rechtsman, J. M. Zeuner, Y. Plotnik, Y. Lumer, D. Podolsky, F. Dreisow, S. Nolte, M. Segev, and A. Szameit, Photonic Floquet topological insulators, Nature (London) **496**, 196 (2013).

[2] L. J. Maczewsky, J. M. Zeuner, S. Nolte, and A. Szameit, Observation of photonic anomalous Floquet topological insulators, Nat. Commun. **8**, 13756 (2017).

[3] Q. Cheng, Y. Pan, H. Wang, C. Zhang, D. Yu, A. Gover, H. Zhang, T. Li, L. Zhou, and S. Zhu, Observation of Anomalous π Modes in Photonic Floquet Engineering, Phys. Rev. Lett. **122**, 173901 (2019).

[4] K. Wintersperger, C. Braun, F. N. Ünal, A. Eckardt, M. D. Liberto, N. Goldman, I. Bloch, and M. Aidelsburger, Realization of anomalous Floquet topological phases with ultracold atoms, Nat. Phys. **16**, 1058 (2020).

[5] Y. H. Wang, H. Steinberg, P. Jarillo-Herrero, and N. Gedik, Observation of Floquet-Bloch states on the surface of a topological insulator, Science **342**, 453 (2013).

[6] J. W. McIver, B. Schulte, F. U. Stein, T. Matsuyama, G. Jotzu, G. Meier, and A. Cavalleri, Light-induced anomalous Hall effect in graphene, Nat. Phys. **16**, 38 (2020).

[7] L. Zhou and J. Gong, Recipe for creating an arbitrary number of Floquet chiral edge states, Phys. Rev. B **97**, 245430 (2018).

[8] H. H. Yap, L. Zhou, J. Wang, and J. Gong, Computational study of the two-terminal transport of Floquet quantum Hall insulators, Phys. Rev. B **96**, 165443 (2017).

[9] H. H. Yap, L. Zhou, C. H. Lee, and J. Gong, Photoinduced half-integer quantized conductance plateaus in topological-insulator/superconductor heterostructures, Phys. Rev. B **97**, 165142 (2018).

[10] Q. Tong, J. An, J. Gong, H. Luo, and C. H. Oh, Generating many Majorana modes via periodic driving: A superconductor model, Phys. Rev. B **87**, 201109(R) (2013).

[11] L. Zhou and J. Gong, Floquet topological phases in a spin-1/2 double kicked rotor, Phys. Rev. A **97**, 063603 (2018).

[12] L. Zhou and Q. Du, Floquet topological phases with fourfold-degenerate edge modes in a driven spin-1/2 Creutz ladder, Phys. Rev. A **101**, 033607 (2020).

[13] R. W. Bomantara and J. Gong, Simulation of Non-Abelian Braiding in Majorana Time Crystals, Phys. Rev. Lett. **120**, 230405 (2018).

[14] R. W. Bomantara and J. Gong, Quantum computation via Floquet topological edge modes, Phys. Rev. B **98**, 165421 (2018).

[15] J. Gong and Q.-H. Wang, Piecewise adiabatic following in non-Hermitian cycling, Phys. Rev. A **97**, 052126 (2018).

[16] J. Gong and Q. Wang, Piecewise adiabatic following: General analysis and exactly solvable models, Phys. Rev. A **99**, 012107 (2019).

[17] L. Zhou and J. Gong, Non-Hermitian Floquet topological phases with arbitrarily many real-quasienergy edge states, Phys. Rev. B **98**, 205417 (2018).

[18] L. Zhou and J. Pan, Non-Hermitian Floquet topological phases in the double-kicked rotor, Phys. Rev. A **100**, 053608 (2019).

[19] L. Zhou, Dynamical characterization of non-Hermitian Floquet topological phases in one dimension, Phys. Rev. B **100**, 184314 (2019).

[20] L. Zhou, Non-Hermitian Floquet phases with even-integer topological invariants in a periodically quenched two-leg ladder, Entropy **22**, 746 (2020).

[21] M. Li, X. Ni, M. Weiner, A. Alù, and A. B. Khanikaev, Topological phases and nonreciprocal edge states in non-Hermitian Floquet insulators, Phys. Rev. B **100**, 045423 (2019).

[22] C. Yuce, PT symmetric Floquet topological phase, Eur. Phys. J. D **69**, 184 (2015).

[23] E. N. Blose, Floquet topological phase in a generalized PT-symmetric lattice, Phys. Rev. B **102**, 104303 (2020).

[24] A. K. Harter and N. Hatano, Real edge modes in a Floquet-modulated PT-symmetric SSH model, arXiv:2006.16890.

[25] J. Pan and L. Zhou, Non-Hermitian Floquet second order topological insulators in periodically quenched lattices, Phys. Rev. B **102**, 094305 (2020).

[26] L. Zhou, Non-Hermitian Floquet topological superconductors with multiple Majorana edge modes, Phys. Rev. B **101**, 014306 (2020).

[27] Z. Yang, Q. Yang, J. Hu, and D. E. Liu, Dissipative Floquet Majorana modes in proximity-induced topological superconductors, arXiv:2004.14918.

[28] M. T. van Caspel, S. E. T. Arze, and I. P. Castillo, Dynamical signatures of topological order in the driven-dissipative Kitaev chain, SciPost Phys. **6**, 026 (2019).

[29] P. He and Z.-H. Huang, Floquet-engineering and simulating exceptional rings with a quantum spin system, Phys. Rev. A **102**, 062201 (2020).

[30] M. S. Rudner and L. S. Levitov, Topological Transition in a Non-Hermitian Quantum Walk, Phys. Rev. Lett. **102**, 065703 (2009).

[31] L. Xiao, X. Zhan, Z. H. Bian, K. K. Wang, X. Zhang, X. P. Wang, J. Li, K. Mochizuki, D. Kim, N. Kawakami, W. Yi, H. Obuse, B. C. Sanders, and P. Xue, Observation of topological edge states in parity time-symmetric quantum walks, Nat. Phys. **13**, 1117 (2017).

[32] X. Zhan, L. Xiao, Z. Bian, K. Wang, X. Qiu, B. C. Sanders, W. Yi, and P. Xue, Detecting Topological Invariants in Nonunitary Discrete-Time Quantum Walks, Phys. Rev. Lett. **119**, 130501 (2017).

[33] K. Wang, X. Qiu, L. Xiao, X. Zhan, Z. Bian, B. C. Sanders, W. Yi, and P. Xue, Observation of emergent momentum-time skyrmions in parity-time-symmetric non-unitary quench dynamics, Nat. Commun. **10**, 2293 (2019).

[34] C. H. Lee and S. Longhi, Ultrafast and anharmonic Rabi oscillations between non-Bloch bands, Commun. Phys. **3**, 147 (2020).

[35] E. J. Bergholtz, J. C. Budich, and F. K. Kunst, Exceptional topology of non-Hermitian systems, arXiv:1912.10048.

[36] Y. Ashida, Z. Gong, and M. Ueda, Non-Hermitian physics, Review article commissioned by *Advances in Physics*, arXiv:2006.01837.

[37] V. M. Martinez Alvarez, J. E. Barrios Vargas, M. Berdakin, and L. E. F. Foa Torres, Topological states of non-Hermitian systems, Eur. Phys. J. Special Topics **227**, 1295 (2018).

[38] S. Yao and Z. Wang, Edge States and Topological Invariants of Non-Hermitian Systems, Phys. Rev. Lett. **121**, 086803 (2018).

[39] S. Yao, F. Song, and Z. Wang, Non-Hermitian Chern Bands, Phys. Rev. Lett. **121**, 136802 (2018).

[40] F. Song, S. Yao, and Z. Wang, Non-Hermitian Topological Invariants in Real Space, Phys. Rev. Lett. **123**, 246801 (2019).

[41] K. Yokomizo and S. Murakami, Non-Bloch Band Theory of Non-Hermitian Systems, Phys. Rev. Lett. **123**, 066404 (2019).

[42] C. H. Lee and R. Thomale, Anatomy of skin modes and topology in non-Hermitian systems, Phys. Rev. B **99**, 201103(R) (2019).

[43] L. Li, C. H. Lee, and J. Gong, Geometric characterization of non-Hermitian topological systems through the singularity ring in pseudospin vector space, Phys. Rev. B **100**, 075403 (2019).

[44] N. Okuma, K. Kawabata, K. Shiozaki, and M. Sato, Topological Origin of Non-Hermitian Skin Effects, Phys. Rev. Lett. **124**, 086801 (2020).

[45] K. Zhang, Z. Yang, and C. Fang, Correspondence between Winding Numbers and Skin Modes in Non-Hermitian Systems, Phys. Rev. Lett. **125**, 126402 (2020).

[46] C. H. Lee, L. Li, and J. Gong, Hybrid Higher-Order Skin-Topological Modes in Non-Reciprocal Systems, Phys. Rev. Lett. **123**, 016805 (2019).

[47] L. Li, C. H. Lee, S. Mu, and J. Gong, Critical non-Hermitian skin effect, Nat. Commun. **11**, 5491 (2020).

[48] D. S. Borgnia, A. J. Kruchkov, and R.-J. Slager, Non-Hermitian Boundary Modes and Topology, Phys. Rev. Lett. **124**, 056802 (2020).

[49] C. H. Lee, L. Li, R. Thomale, and J. Gong, Unraveling non-Hermitian pumping: Emergent spectral singularities and anomalous responses, Phys. Rev. B **102**, 085151 (2020).

[50] X. Zhang and J. Gong, Non-Hermitian Floquet topological phases: Exceptional points, coalescent edge modes, and the skin effect, Phys. Rev. B **101**, 045415 (2020).

[51] J. K. Asbóth, Symmetries, topological phases, and bound states in the one-dimensional quantum walk, Phys. Rev. B **86**, 195414 (2012).

[52] J. K. Asbóth and H. Obuse, Bulk-boundary correspondence for chiral symmetric quantum walks, Phys. Rev. B **88**, 121406(R) (2013).

[53] See Supplemental Material at http://link.aps.org/supplemental/10.1103/PhysRevB.103.L041404 for the explicit expressions of the quasienergy dispersion $E(k)$ and effective Hamiltonian components $[h_{\alpha x}(k), h_{\alpha y}(k)]$ in Sec. I; Sec. II for more examples of the bulk topological phase diagram; Sec. III for another example of the static spin textures and dynamic winding numbers; Sec. IV for explicit expressions of the system Hamiltonian under the OBC; Sec. V for details about the Q-matrix in static non-Hermitian systems; Sec. VI for other examples of the Floquet spectrum and OBWNs; Sec. VII for the profiles of bulk Floquet skin modes and edge states; and Sec. VIII for the generalization of winding number w_α to multiple band cases.

[54] Z. Gong, Y. Ashida, K. Kawabata, K. Takasan, S. Higashikawa, and M. Ueda, Topological Phases of Non-Hermitian Systems, Phys. Rev. X **8**, 031079 (2018).

[55] K. Kawabata, K. Shiozaki, M. Ueda, and M. Sato, Symmetry and Topology in Non-Hermitian Physics, Phys. Rev. X **9**, 041015 (2019).

[56] H. Zhou and J. Y. Lee, Periodic table for topological bands with non-Hermitian symmetries, Phys. Rev. B **99**, 235112 (2019).

[57] B. Zhu, Y. Ke, H. Zhong, and C. Lee, Dynamic winding number for exploring band topology, Phys. Rev. Research **2**, 023043 (2020).

[58] L. Zhang, L. Zhang, and X. Liu, Unified Theory to Characterize Floquet Topological Phases by Quench Dynamics, Phys. Rev. Lett. **125**, 183001 (2020).

[59] D. C. Brody, Biorthogonal quantum mechanics, J. Phys. A: Math. Theor. **47**, 035305 (2014).

[60] J. Song and E. Prodan, AIII and BDI topological systems at strong disorder, Phys. Rev. B **89**, 224203 (2014).

[61] I. Mondragon-Shem, T. L. Hughes, J. Song and E. Prodan, Topological Criticality in the Chiral-Symmetric AIII Class at Strong Disorder, Phys. Rev. Lett. **113**, 046802 (2014).

[62] A. Kitaev, Anyons in an exactly solved model and beyond, Ann. Phys. (Amsterdam) **321**, 2 (2006).

[63] The parts falling on the horizontal axis in Δ_0 and Δ_π of Fig. 4 correspond to Floquet topological edge states with real eigenphases $E = 0$ and $E = \pi$, which only appear under the open-boundary condition.